Laser ablation inductively coupled plasma mass spectrometry as a novel clinical imaging tool to detect asbestos fibres in malignant mesothelioma.

VOLOACA, Oana M., GREENHALGH, Calum J., COLE, Laura <http://orcid.org/0000-0002-2538-6291>, CLENCH, Malcolm R. <http://orcid.org/0000-0002-0798-831X>, MANAGH, Amy J. <http://orcid.org/0000-0003-1479-0843> and HAYWOOD-SMALL, Sarah <http://orcid.org/0000-0002-8374-9783>

Published version

VOLOACA, Oana M., GREENHALGH, Calum J., COLE, Laura, CLENCH, Malcolm R., MANAGH, Amy J. and HAYWOOD-SMALL, Sarah (2020). Laser ablation inductively coupled plasma mass spectrometry as a novel clinical imaging tool to detect asbestos fibres in malignant mesothelioma. Rapid Communications in Mass Spectrometry, 34 (21), e8906.

Copyright and re-use policy

Received: 21 May 2020 | Revised: 21 July 2020 | Accepted: 22 July 2020

DOI: 10.1002/rcm.8906

Rapid Communications in Mass Spectrometry WILEY

RESEARCH ARTICLE

Laser ablation inductively coupled plasma mass spectrometry as a novel clinical imaging tool to detect asbestos fibres in malignant mesothelioma

Oana M. Voloaca[1] | Calum J. Greenhalgh[2] | Laura M. Cole[1] | Malcolm R. Clench[1] | Amy J. Managh[2] | Sarah L. Haywood-Small[1]

[1]Biomolecular Research Centre, Sheffield Hallam University, City Campus, Howard Street, Sheffield, S1 1WB, UK

[2]Department of Chemistry, Loughborough University, Loughborough, LE11 3TU, UK

Correspondence
S. L. Haywood-Small, Biomolecular Research Centre, Sheffield Hallam University, City Campus, Howard Street, Sheffield S1 1WB, UK.
Email: s.haywood-small@shu.ac.uk

A. J. Managh, Department of Chemistry, Loughborough University, Loughborough LE11 3TU, UK.
Email: a.j.managh@lboro.ac.uk

Rationale: Malignant pleural mesothelioma is an extremely aggressive and incurable malignancy associated with prior exposure to asbestos fibres. Difficulties remain in relation to early diagnosis, notably due to impeded identification of asbestos in lung tissue. This study describes a novel laser ablation inductively coupled plasma mass spectrometry (LA-ICP-MS) imaging approach to identify asbestos within mesothelioma models with clinical significance.

Methods: Human mesothelioma cells were exposed to different types of asbestos fibres and prepared on plastic slides for LA-ICP-MS analysis. No further sample preparation was required prior to analysis, which was performed using an NWR Image 266 nm laser ablation system coupled to an Element XR sector-field ICP mass spectrometer, with a lateral resolution of 2 μm. Data was processed using LA-ICP-MS ImageTool v1.7 with the final graphic production made using DPlot software.

Results: Four different mineral fibres were successfully identified within the mesothelioma samples based on some of the most abundant elements that make up these fibres (Si, Mg and Fe). Using LA-ICP-MS as an imaging tool provided information on the spatial distribution of the fibres at cellular level, which is essential in asbestos detection within tissue samples. Based on the metal counts generated by the different types of asbestos, different fibres can be identified based on shape, size, and elemental composition. Detection of Ca was attempted but requires further optimisation.

Conclusions: Detection of asbestos fibres in lung tissues is very useful, if not necessary, to complete the pathological dt9iagnosis of asbestos-related malignancies in the medicolegal field. For the first time, this study demonstrates the successful application of LA-ICP-MS imaging to identify asbestos fibres and other mineral fibres within mesothelioma samples. Ultimately, high-resolution, fast-speed LA-ICP-MS analysis has the potential to be integrated into clinical workflow to aid earlier detection and stratification of mesothelioma patient samples.

1 | INTRODUCTION

Malignant pleural mesothelioma (MPM) is a rare, extremely aggressive and incurable malignancy associated with occupational and environmental exposure to asbestos and other mineral fibres (MF).[1] MPM has a long latency period with an average of 30–60 years, with a median survival time of 6–12 months and a 5-year survival of <5%.[2] Despite asbestos being banned in most Western countries, the global incidence of MPM is expected to increase over the next two decades, mainly due to the long latency period, continuous mining and usage in certain countries, as well as environmental exposure.[1] Difficulties remain in relation to presymptomatic diagnosis, particularly due to lack of validated biomarkers and impeded identification of asbestos fibres in lung tissue.[2] Being able to accurately identify these MF within samples is not only essential in aiding early diagnosis of MPM, but it also plays a key role in linking this diagnosis to asbestos exposure, which has high implications in legal, social and political matters.[3]

Asbestos is an umbrella term that comprises various polyfilamentous silicate minerals, which, once broken into fibrils, can be easily inhaled, in most cases lodging into the lining of the lungs and triggering a chronic inflammatory cascade.[2] Asbestos consists of two main classes; the serpentines (of which chrysotile is the most common type) and the amphiboles, including crocidolite, amosite, tremolite, anthophyllite and actinolite.[4] The potency of these MF to induce asbestos-related diseases (ARD), such as asbestosis, lung cancer and MPM, varies based on their differences in chemical and physical structures, presented briefly in Table 1.

By geological classification, asbestos fibres are defined as having aspect ratio ≥3:1, length ≥5 μm, and width <0.25 μm.[6] This does not account for cleavage fragments, or high potency shorter fibres.[9] This asbestos classification was created to facilitate the counting of the MF using standard microscopy methods and was not based on the potency of these segments or shorter fibres to induce ARD.[10]

According to the latest guidelines published by the British Thoracic Society, the current investigation workflow involves an urgent chest X-ray of symptomatic patients, followed by a pleural evaluation computerised tomography (CT) scan, immunohistochemistry of biopsies or cytology-type specimens, and establishing the prospect of occupational exposure or para exposure to asbestos fibres.[11] However, it is essential to detect MF in lung tissues to complete the pathological diagnosis of MPM in correlation to asbestos exposure. The routine quantification method uses phase contrast microscopy to count only the fibres that adhere to the definition mentioned above. Therefore, current test methods exclude certain types of MF such as cleavage fragments, short or thin fibres, or naturally occurring MF (e.g. erionite), despite all of these being previously reported to cause ARD.[9,12,13]

More established methods of asbestos identification and quantification, such as scanning electron microscopy (SEM) and transmission electron microscopy (TEM), generally employ chemical digestion of the tissues in order to eliminate the organic matrix, thus losing all the spatial information offered by imaging methods such as optical and polarised light microscopy.[14] However, these imaging methods cannot differentiate between asbestiform and non-asbestiform fibres and fail to detect low concentrations of MF or fibres that are less than 0.20 μm in diameter.[3] Moreover, methods of differentiating MF based on surface charge are not relatable since non-asbestiform amphiboles are virtually identical to asbestiform amphibole fibres in morphology, crystal structure, refractive index, and chemical composition.[9]

Given the similarities in chemical structures between the MF (i.e. silicates), and also the proportional discrepancies of main elements such as Fe, Ca and Mg between each fibre type, elemental analysis has gained popularity in recent years compared with optical

TABLE 1 Classification, common names and physicochemical properties of the mineral fibres used in this work

Technical name	Common name	Nominal composition	Chemical properties	Physical properties
Serpentine				
Chrysotile[5]	White asbestos	$Mg_3[Si_2O_5](OH)_4$	Two-layered silicate (one tetrahedral and one octahedral layer), with a hollow central core. Positive surface charge. Degradable in dilute acids.	Curled. Length: several mm to more than 10 cm. Flexible fibres
Amphiboles				
Crocidolite[6]	Blue asbestos	$Fe_2H_{16}Mg_3Na_2O_{24}Si_8^{+14}$	Double-chain silicate, resistant to acids, negative surface charge in water.	Shorter, thinner, flexible fibres. Less heat resistant.
Amosite[7]	Brown asbestos	$Mg_{1.5}Fe^{2+}{}_{5.5}[Si_8O_{22}](OH)_2$	Double-chain silicate, can be resistant to acids, negative surface charge in water.	Long, straight, coarse fibres. Can be flexible.
Non-asbestiform				
Wollastonite[8]	Unspecified	$CaSiO_3$	Soluble in concentrated HCl. Composed of chains of silica tetrahedra connected side by side through calcium.	Bladed crystal masses, single crystals can show an acicular particle shape and usually it exhibits a white colour

methods. One of the first reports used an in-air micro-particle induced X-ray emission (in-air micro-PIXE) system to identify the location of asbestos bodies in lung tissue sections.[15] However, this has only been achieved with limited spatial resolution. Sub-micrometer lateral resolution has been reported in a study by Pascolo et al who employed soft X-ray imaging and X-ray fluorescence (XRF) microscopy to investigate elemental lateral distribution of asbestos bodies in lung tissue.[16] Given the complexity of the techniques used in the study, the limitations revolve around the applicability in a clinical setting and it is presented more as a research tool on chemical interactions between fibres and cells.

Laser ablation inductively coupled plasma mass spectrometry (LA-ICP-MS) is one of the most versatile techniques for the analysis of trace elemental distribution due to its exceptional limits of detection for a vast range of metallic analytes ($\mu g\,g^{-1}$), ease of sample preparation, excellent lateral resolution and relatively good acquisitions times, making it the ideal candidate for clinical settings. Furthermore, due to technical advancements in instrumentation, cellular analysis with a relatively short time of acquisition is possible. It has gained popularity in recent years and it is continuing to develop through the introduction of novel chamber designs and geometries. For example, earlier designs allowed for resolutions between 5 and 100 μm[17] compared with recent advancements capable of cellular analysis with 1–2 μm spot size[18,19] or even sub-micrometre spot diameter recently reported by Vanhaecke et al.[20] Given these features, LA-ICP-MS imaging is an established technique in monitoring elemental distribution in certain neurodegenerative conditions such as Alzheimer's disease[21] and Parkinson's disease.[22] LA-ICP-MS has also been employed as an imaging tool in cancer research[23] and as a drug monitoring tool.[24]

To our knowledge, this is the first application of LA-ICP-MS imaging to spatially resolve asbestos and other MF at cellular resolution. We aimed to identify some of the most common MF, amosite, chrysotile and crocidolite, as well as a non-asbestiform control, wollastonite, within MPM models using a laser ablation system that consists of a dual-volume ablation cell with an integrated ICP torch, which allows for an increase in absolute sensitivity and faster analysis times.[18] Preliminary data on cellular models presented herein suggest that LA-ICP-MS has the potential to identify and differentiate between various asbestos types in different biological samples. This study highlights the findings of current research efforts concerning the use of LA-ICP-MS as a novel clinical imaging tool to detect asbestos fibres. Further studies will be required to validate the approach in human lung tissue samples.

2 | EXPERIMENTAL

2.1 | Cell culture

Human mesothelioma cells, NCI-H28, were purchased from the American Type Culture Collection (ATCC) (LGC, Teddington, UK) and were grown in complete RPMI 1640 medium (10% v/v heat-inactivated fetal bovine serum and 1% v/v penicillin/streptomycin) at 37°C in a humidified atmosphere with 5% CO_2. The cells were cultured and harvested according to established cell culture protocols. All cell culture materials were supplied by Gibco (Life Technologies, Carlsbad, CA, USA). The cell line was confirmed to be negative for mycoplasma every 3 months using the MycoAlert™ mycoplasma detection kit (LONZA, Basel, Switzerland).

2.2 | Mineral fibres

The Union for International Cancer Control (UICC) standard asbestos fibres were supplied by the Health and Safety Laboratory (Buxton, UK) and were kindly donated by Santia Asbestos Management Ltd (Mansfield, UK). All the asbestos types were research-grade, UICC-accredited fibres. The panel included amosite, chrysotile, crocidolite, and a non-asbestiform fibre, wollastonite. The fibres were weighed and handled only in specially designed laminar flow hoods (Santia Asbestos Management Ltd) until they were prepared in phosphate-buffered saline (PBS) solutions to a stock concentration of 1 mg/mL. Once in solution, the fibres pose a low risk of inhalation. The asbestos fibre solutions were sterilised at 121°C in an autoclave and stored at room temperature. Prior to treatment, the solutions were passed through a 22-gauge needle five times to ensure separation of the fibrils.

2.3 | Sample preparation

NCI-H28 cells (10×10^4 cells/well) were seeded in six-well plates and allowed to adhere to the bottom of the wells for 24 h, before being treated with 3 μg/mL of single-type asbestos solutions. After 24 h, cells were harvested and counted (5×10^4 cells/mL). Cytospins were prepared onto plastic slides by centrifugation at 100 *g* for 3 min. The slides were kept at −80°C until LA-ICP-MS analysis. No further sample preparation was needed prior to ablation.

2.4 | LA-ICP-MS imaging

Analysis was performed using an NWR Image 266 nm laser ablation system (Elemental Scientific Lasers, Bozeman, MT, USA) coupled to an Element XR sector-field ICP mass spectrometer (Thermo Scientific, Bremen, Germany).[25] The laser ablation system used consists of a two-volume ablation cell and dual concentric injector (DCI).[18] A helium gas flow at 1.45 L min^{-1} was used through the ablation chamber, with an argon flow of 0.475 L min^{-1} introduced through the DCI. A laser spot diameter of 2 μm, 20 Hz repetition frequency, 40 μm s^{-1} scan speed and ~18 J cm^{-2} fluence were used during ablation. Ablated lines were parallel to each other with no gaps between the lines to ensure full ablation of the area. A 2-s laser warmup period and 2-s washout time were allowed before and after each line. LA-ICP-MS parameters were optimised for maximum ^{24}Mg, ^{29}Si, ^{57}Fe ion

sensitivity, while ensuring that individual pulse responses could be resolved at the stated repetition frequency. These elements were imaged separately, due to the slow scanning speed of the ICP-MS instrument compared with the fast response of the laser ablation system. A P7882 photon counter board (FAST ComTec GmbH, Oberhaching, Germany) was connected to the ion detection board of the mass spectrometer to collect the data and the signal was monitored using MCDWIN software (FAST ComTec GmbH) as described previously.[26] This allowed for blind time free collection of the data using a 10-ms dwell time. Data processing was performed using in-house software, LA-ICP-MS ImageTool v1.7 (Reid-IT Ltd, Loughborough, UK),[27] with the final graphic production made using DPlot (Hydesoft Computing, Vicksburg, MS, USA).

3 | RESULTS AND DISCUSSION

To assess the potential of LA-ICP-MS to be ultimately integrated within the clinical setting as a MF imaging tool for patients suspected of MPM, preliminary studies had first to be carried out on cell lines exposed to MF.

In this work, chrysotile, amosite, crocidolite and wollastonite were selected on the panel of MF to be detected based on the metal content. The panel was carefully selected to include both the most common type of asbestos (i.e. chrysotile),[2] and the MF with the highest carcinogenicity and bioresistance (i.e. crocidolite).[6] The MF were identified by LA-ICP-MS based on the Fe, Mg and Si content. Method optimisation included the selection of the right isotopes for

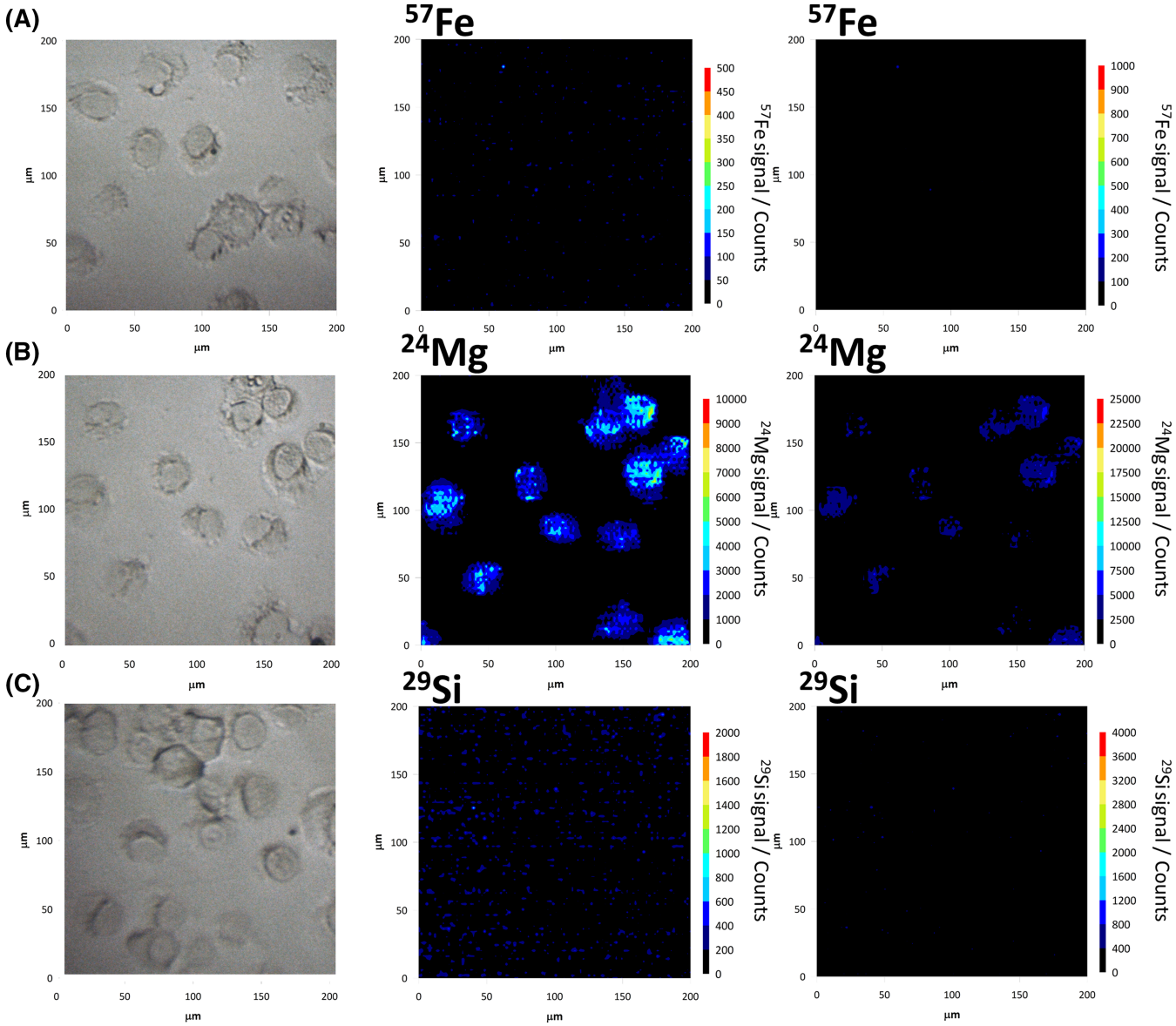

FIGURE 1 NCI-H28 cells cultured in a fibre-free environment. Left column shows the microscope perspective of the areas prior to ablation. Middle column presents the elemental distribution as analysed by LA-ICP-MS imaging. Intensity bar was adjusted in the right-hand column to normalise against the cellular background. A, Low ^{57}Fe distribution within the mesothelioma cells; B, high ^{24}Mg intensity counts ; C, the significantly low overall ^{29}Si content in NCI-H28 cells [Color figure can be viewed at wileyonlinelibrary.com]

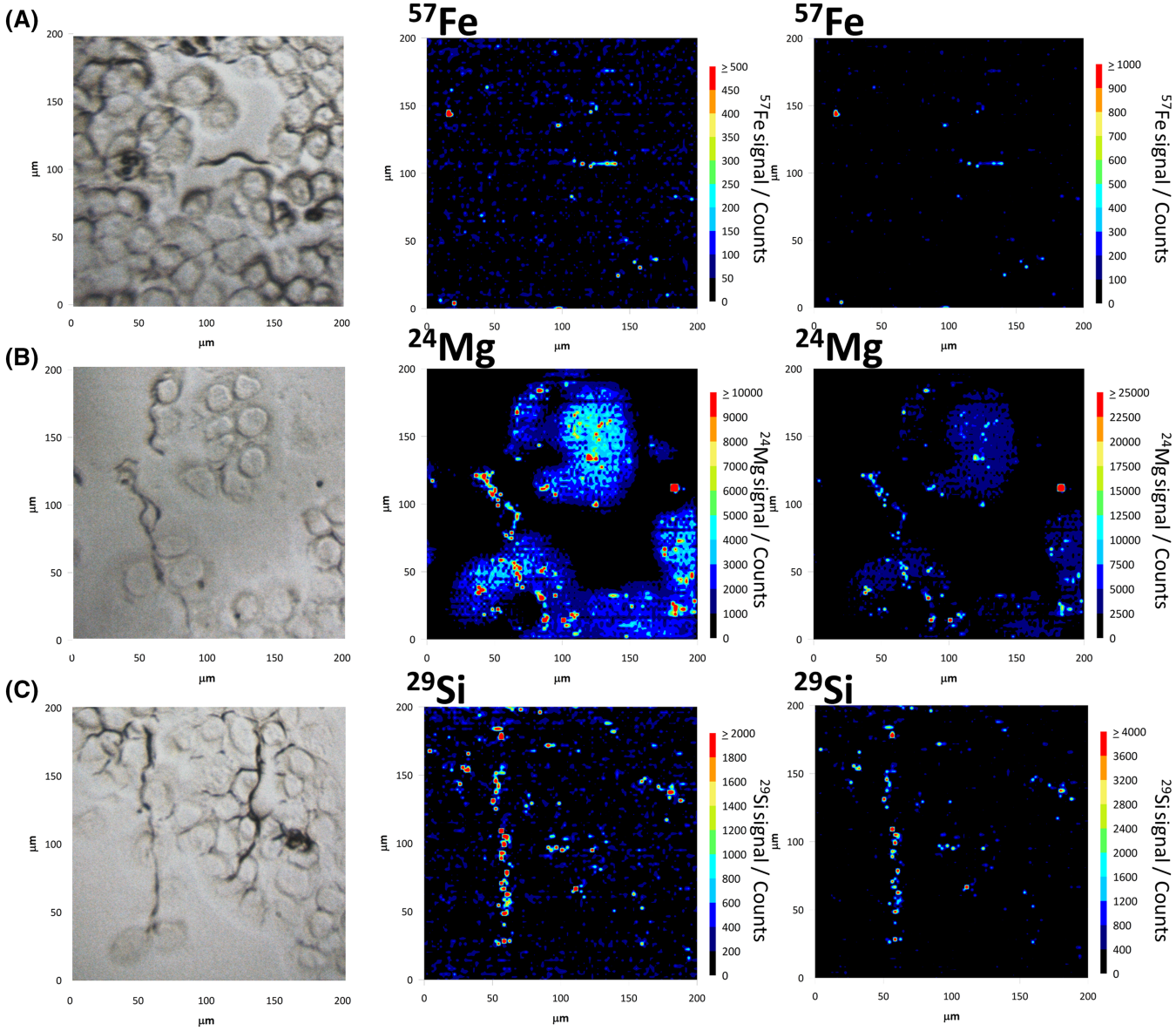

FIGURE 2 NCI-H28 monolayer cultured with chrysotile. Left column shows the microscope perspective of the areas prior to ablation. Areas with fibres visible using optical microscopy were selected for proof of concept. Note the physical aspect of the fibres typical for chrysotile. Middle column presents the elemental distribution as analysed by LA-ICP-MS imaging. The intensity bar was adjusted in the right-hand column to focus on the fibres. A, the low ^{57}Fe distribution within the sample. Chrysotile is known for its limited iron content and this is reflected in the metal counts. B The relatively high ^{24}Mg intensity signal in the fibres visible in microscope images, as well as smaller fragments within the cell layer that could not be seen initially. C, Similarly, the ^{29}Si distribution within the matrix and chrysotile fibres. LA-ICP-MS preserves the curly shapes of the chrysotile fibrils [Color figure can be viewed at wileyonlinelibrary.com]

each element. First, mapping the iron distribution within biological samples has proven difficult due to common interferences of ^{56}Fe with the plasma gas.[28] For this study, ^{57}Fe proved to be a valuable alternative, offering above-background signals for all the asbestos fibres used. Secondly, ^{24}Mg, the most abundant stable isotope of magnesium, was selected after method optimisation, generating high signals for all sample types. Finally, regardless of whether they are classified as carcinogenic asbestiform fibres, all MF are silicates and therefore detection of silicon was a key step. To avoid the interferences caused by the high silicon content in glass slides, all samples were prepared on plastic slides. Analysis was optimised for the best signal intensity of MF. Despite being the second most abundant isotope, ^{29}Si generated signals above the background noise, allowing clear identification of all MF. Of the other major matrix components, oxygen is undetectable via ICP-MS, while ^{40}Ca and ^{44}Ca analysis was attempted but was unsuccessful due to high interferences from the plasma gas (data not shown). The colour intensity scale in the LA-ICP-MS images can be adjusted to display

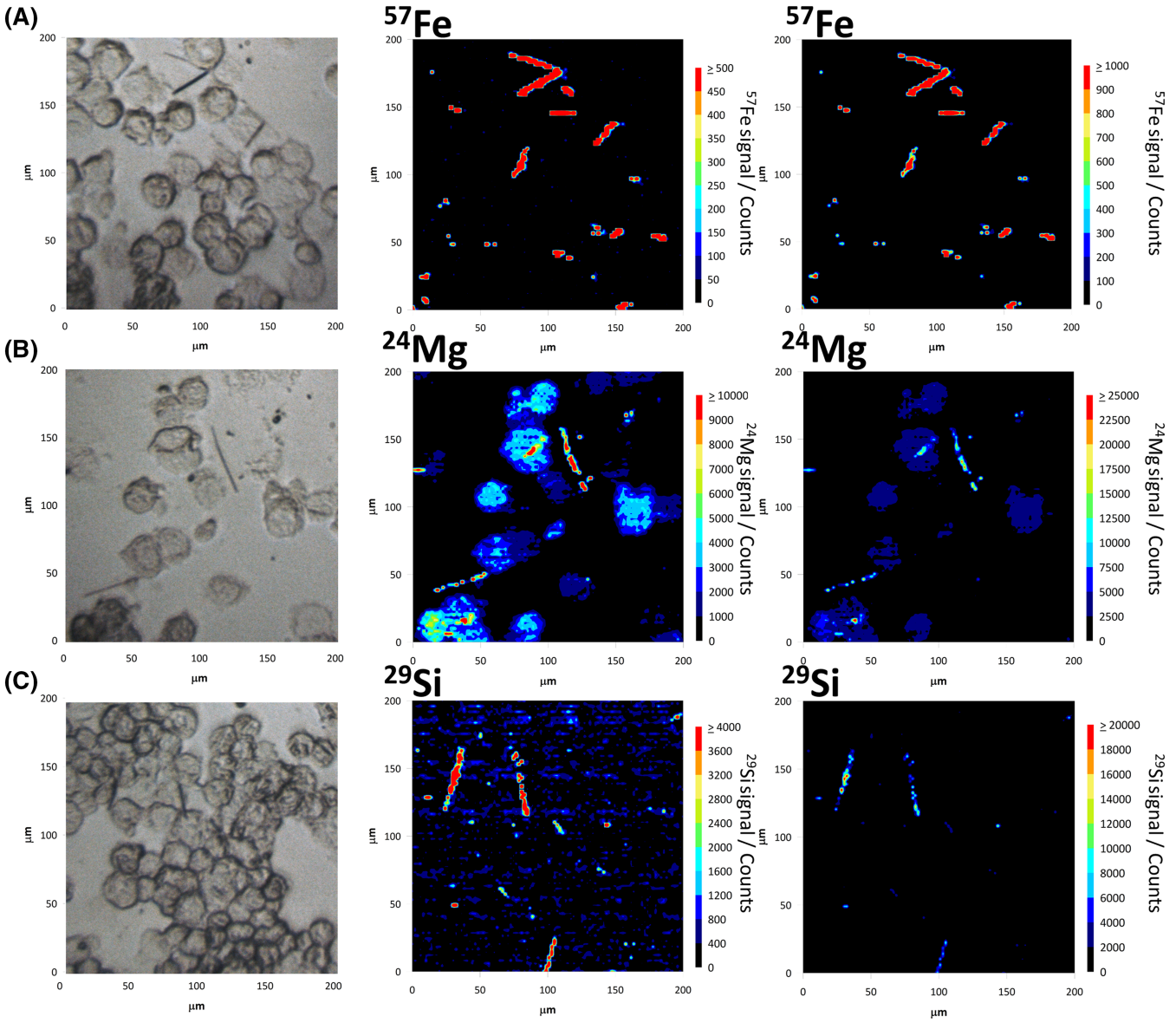

FIGURE 3 NCI-H28 cells cultured with amosite fibres. Left column shows the microscope perspective of the areas prior to ablation. Areas with fibres visible using optical microscopy were selected for proof of concept. Middle column presents the elemental distribution as analysed by LA-ICP-MS imaging. The intensity bar was adjusted in the right-hand column to focus on the fibres. As expected, higher ^{57}Fe distribution is presented in (A) than for serpentine fibres. Note the shorter fibres and fibre amosite fibre fragments spread all over the sample as shown using LA-ICP-MS imaging. B, The ^{24}Mg counts within the sample. Note that the engulfed amosite fibres are not visible in the microscopic image. C, ^{29}Si distribution within the matrix and amosite fibres [Color figure can be viewed at wileyonlinelibrary.com]

the full signal range of the fibres. In these data the intensity scale was kept consistent between samples and the background signal from the cells was removed from the images in order to facilitate easier identification of fibres.

3.1 | Untreated

NCI-H28 cells are a well-established model for epithelioid MPM, the most prevalent type of mesothelioma (75–80% cases),[2] and provided a biologically relevant matrix for the MF. Analysis was therefore carried out initially on two-dimensional (2D) cell models in order to ensure that the elemental signals provided by the MF were above the cellular background before moving on to more biologically complex samples. To assess whether different types of MPM would give different signal backgrounds, a biphasic cell line, MSTO-211H, was also used as a matrix (data not presented). There was no significant difference in either ^{24}Mg, ^{57}Fe or ^{29}Si intensity signals generated by the two cellular models. The elemental intensity generated by the NCI-H28 cells is presented in Figures 1A–1C. Note the signal

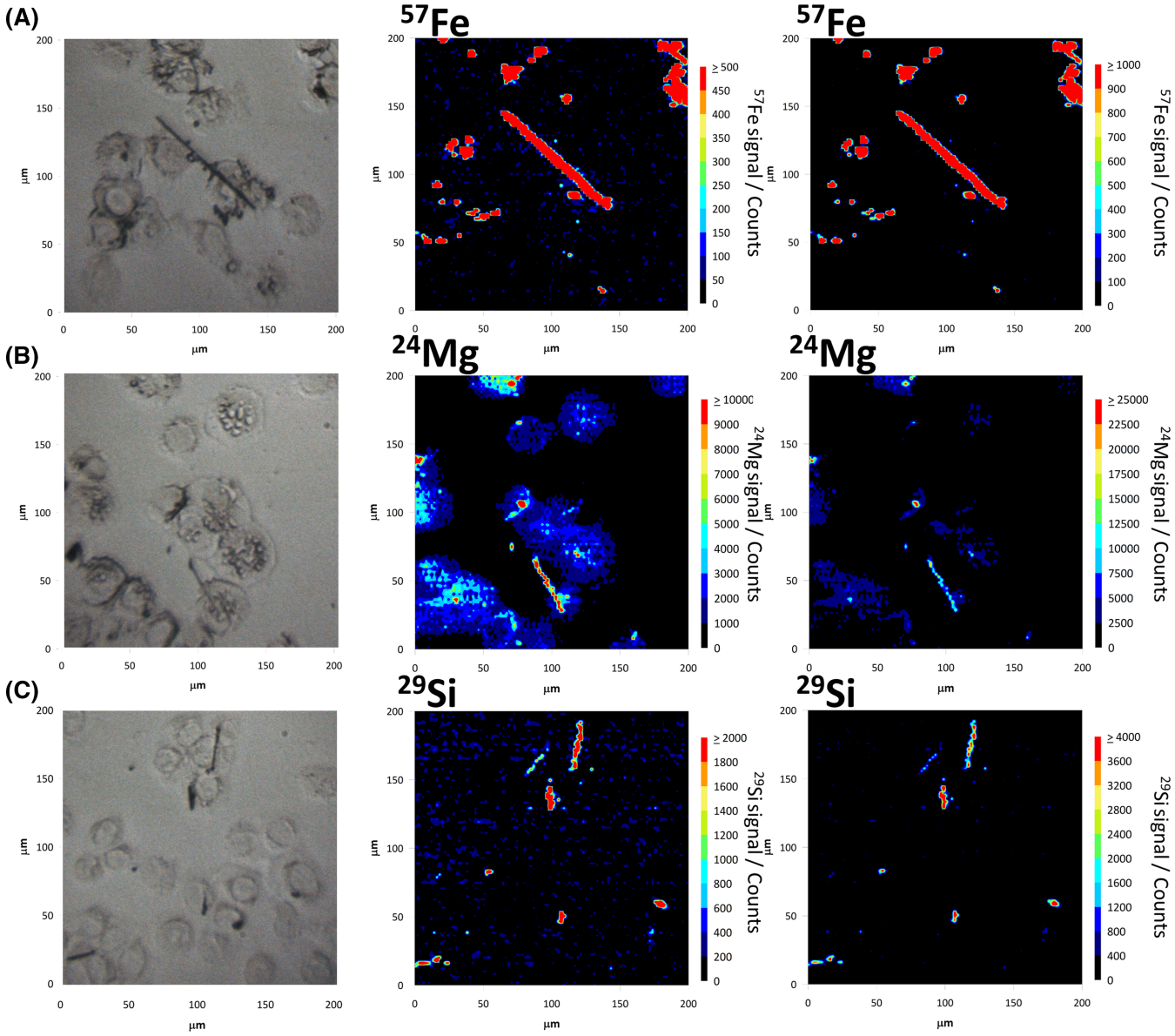

FIGURE 4 NCI-H28 cells cultured with crocidolite fibres. Left-hand column shows the microscope perspective of the areas prior to ablation. Areas with fibres visible using optical microscopy were selected for proof of concept. Middle column presents the elemental distribution as analysed by LA-ICP-MS imaging. The intensity bar was adjusted in the right-hand column to focus on the fibres. The highest ^{57}Fe concentration is presented in (A) which coincides with the nominal composition of crocidolite. ^{24}Mg counts can be seen in (B). Hardly any fibres can be seen in the microscopic images in (C). The LA-ICP-MS images offer information beneath the cellular layer, exposing the crocidolite fibres based on ^{29}Si content [Color figure can be viewed at wileyonlinelibrary.com]

intensity generated by ^{24}Mg (Figure 1B), present at detectable and relatively homogeneous levels within the biological matrix, making it a suitable choice to aid correlation of the LA-ICP-MS and microscopic images.

3.2 | Chrysotile

Chrysotile is known for its long, curled appearance and short biopersistence in the lungs.[5] The slightly decreased carcinogenicity of chrysotile compared with that of other asbestos fibres is mainly attributed to the low iron concentration. Chrysotile contains trace amounts of iron as an impurity (1–6%) where iron atoms replace magnesium in the outer Mg-hydroxide octahedral or silicon in the inner silica tetrahedral.[29] These trace amounts of Fe allow for visualisation of chrysotile fibres and fibre fragments in Figure 2A. As a matrix component of chrysotile, representing 26.31% of its nominal composition, magnesium can be easily detected within the chrysotile long fibres, as well as in shorter fragments (Figure 2B). Another clear example of the long physical appearance of chrysotile can also be noted in Figure 2C. Apart from identification of the single, long fibre, LA-ICP-MS images allow for visualisation of smaller fragments.

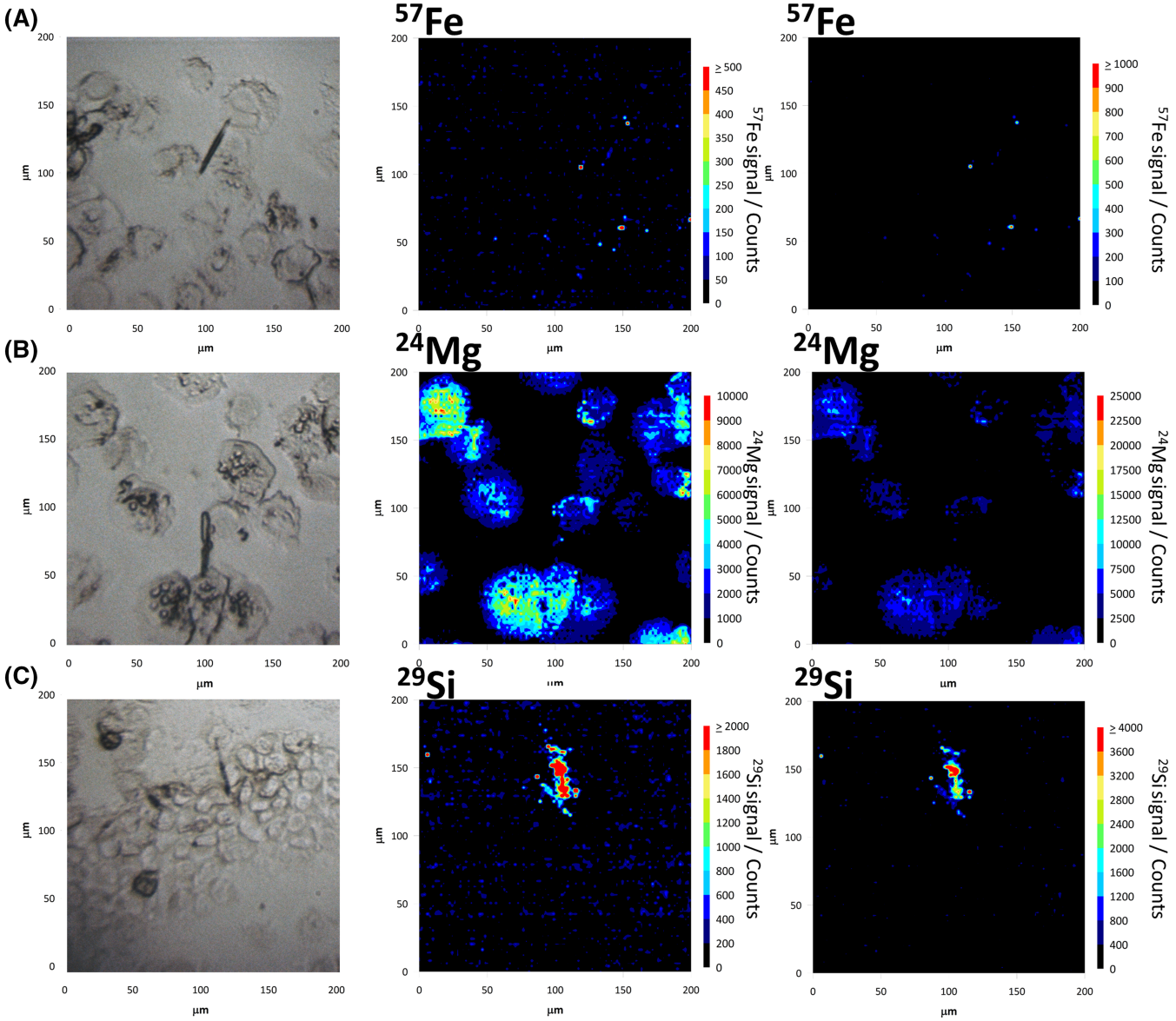

FIGURE 5 NCI-H28 cells cultured with a non-asbestiform control, wollastonite. Left-hand column shows the microscope perspective of the areas prior to ablation. Areas with fibres visible using optical microscopy were selected for proof of concept. Middle column presents the elemental distribution as analysed by LA-ICP-MS imaging. The intensity bar was adjusted in the right-hand column to focus on the fibres. No significant ^{57}Fe and ^{24}Mg signals were given by the wollastonite fibres as presented in the LA-ICP-MS data from (A) and (B). On the other hand, wollastonite is a silicate and was therefore expected to be identified based on the ^{29}Si content. This is shown in (C) where the ^{29}Si distribution corresponds to the wollastonite fibres visible in the optical image on the left [Color figure can be viewed at wileyonlinelibrary.com]

3.3 | Amosite

Amosite asbestos is, chemically speaking, one of the most straightforward MF to be identified by LA-ICP-MS based on Fe, Mg and Si content. Fe represents more than 39% of the nominal composition of amosite, which is reflected in the high signal intensity presented in Figure 3A. Similarly, magnesium is also present, albeit in a smaller percentage, in amosite fibres (Figure 3B). Being a proof of concept study, regions containing visible fibres, as determined by optical microscopy, were selected for analysis. The pre-ablation, corresponding optical images were included in the left-hand columns of the Figures for comparison with the LA-ICP-MS images. It was notable that in cases where fibres disappear within or underneath a cell in the microscopic images, they were still noticeable in the LA-ICP-MS images based upon their metal signal (Figures 3B and 3C). This is an advantage of LA-ICP-MS compared with microscopic methods. It has been reported that MF shorter than 5 µm normally are engulfed by cells through frustrated phagocytosis, whereas longer fibres can become lodged in the internuclear bridge of the cells.[30] Localisation does vary between cell types. In clinical samples and experimental animal models, fibres are usually contained in both fibroblasts and macrophages.[31–33] However, the internalisation of asbestos fibres into various non-phagocytic mesothelial cells has also been

reported by many researchers.[34] Given the sample preparation in this proof of concept study, the localisation of the fibres varies between the samples, supporting the hypothesis that LA-ICP-MS can ablate and detect MF regardless of the positioning. One such example is presented in Figure 3B where a short amosite fibre has been engulfed by the cell, hindering visualisation simply by light microscopy.

3.4 | Crocidolite

Importantly, the difference in nominal composition between the elements that make up each of the MF selected in the panel is mirrored in the intensity generated by analysis. For instance, the Fe content in chrysotile presented earlier in Figure 2A compared with crocidolite (Figure 4A) brings the work a step closer to differentiating between the fibres in blind analysis based solely on elemental composition. As magnesium is a very common impurity in crocidolite, its signal can easily provide spatial information of the position of the crocidolite fibres (Figure 4B). Likewise, a high ^{29}Si signal is shown in Figure 4C, both in longer crocidolite fibres and in the shorter fragments.

3.5 | Wollastonite

Wollastonite was selected as a negative control MF due to its similar chemical and physical properties to those of established asbestos fibres. It is a calcium inosilicate mineral with no established association to MPM. Mined in a similar fashion to other MF, wollastonite might contain other metal impurities including Fe,[8] which could explain the slight ^{57}Fe signal present in Figure 5A. On the other hand, no magnesium was present in the wollastonite samples, as shown by the LA-ICP-MS images (Figure 5B). As expected, a high ^{29}Si signal was generated in the case of this MF (Figure 5C). Notably, some impurities present in the optical image were proven not to be wollastonite, confirming the high sensitivity of this technique.

4 | CONCLUSIONS

The poor treatment response and short-term survival of MPM cases are largely attributed to late diagnosis and lack of a standardised screening method. Moreover, current detection of asbestos fibres by microscopy is inadequate, with numerous fibres being undetectable, even in patients with heavy asbestos exposure.[3]

Our study is the first to use LA-ICP-MS to spatially resolve multiple MF within a cellular background based on the presence of three main elemental components. The use of a low-dispersion ablation cell provided high-resolution, high-speed analysis, demonstrating that LA-ICP-MS has the potential to screen for the presence of asbestos in more biologically complex models such as human tissue samples. Further investigation to look at detection and differentiation of asbestos bodies with different elemental compositions would improve the technique and facilitate identification of fibre subsets. As a proof of concept study, the present work aimed to prove the ability of LA-ICP-MS to detect these MF against a cellular background using a low lateral resolution (2 μm). The work sets the basis for future multi-element analysis carried out using a time-of-flight mass spectrometer, which provides pseudo-simultaneous detection of the full mass range.

We succeeded in mapping amosite, chrysotile, crocidolite and wollastonite distribution within 2D cytospins based on the metal content. Further work will focus on more biologically complex matrices such as 3D models and patient samples to confirm the presence of asbestos. These preliminary data suggest that ultimately this instrument can be used within a clinical setting to aid early diagnosis of MPM and patient outcome.

ACKNOWLEDGEMENTS

This research is supported by the June Hancock Mesothelioma Research Fund. Research grade asbestos fibres were kindly donated by Santia Asbestos Management Ltd. The authors are grateful to Mr James Hough for his early assistance with this research. Clinical support was provided by Professor Suvarna and Dr Kitsanta (Department of Histopathology, Royal Hallamshire Hospital, Sheffield, UK).

PEER REVIEW

The peer review history for this article is available at https://publons.com/publon/10.1002/rcm.8906.

ORCID

Oana M. Voloaca https://orcid.org/0000-0003-0131-6907
Calum J. Greenhalgh https://orcid.org/0000-0002-4904-3234
Laura M. Cole https://orcid.org/0000-0002-2538-6291
Malcolm R. Clench https://orcid.org/0000-0002-0798-831X
Amy J. Managh https://orcid.org/0000-0003-1479-0843
Sarah L. Haywood-Small https://orcid.org/0000-0002-8374-9783

REFERENCES

1. Zhang W, Wu X, Wu L, et al. Advances in the diagnosis, treatment and prognosis of malignant pleural mesothelioma. *Ann Trans Med*. 2015;3:182-189. https://doi.org/10.3978/j.issn.2305-5839.2015.07.03
2. Bononi A, Napolitano A, Pass HI, Yang H, Carbone M. Latest developments in our understanding of the pathogenesis of mesothelioma and the design of targeted therapies. *Expert Rev Respir Med*. 2015;9(5):633-654. https://doi.org/10.1586/17476348.2015.1081066
3. Capella S, Bellis D, Belluso E. Diagnosis of asbestos-related diseases: The mineralogist and pathologist's role in medico-legal field 2016. *Am J Forensic Med Pathol*. 20161;37(1):24-28.
4. Gamble JF, Gibbs GW. An evaluation of the risks of lung cancer and mesothelioma from exposure to amphibole cleavage fragments. *Regul Toxicol Pharmacol*. 2008;52:S154-S186. https://doi.org/10.1016/j.yrtph.2007.09.020
5. Okimoto QF, Jube G, Carbone MG, et al. Continuous exposure to chrysotile asbestos can cause transformation of human mesothelial

cells via HMGB1 and TNF-α signaling. *Am J Pathol*. 2013;183(5):1654-1666. https://doi.org/10.1016/j.ajpath.2013.07.029
6. Andreozzi GB, Pacella A, Corazzari I, Tomatis M, Turci F Surface reactivity of amphibole asbestos: A comparison between crocidolite and tremolite. *Sci Rep* 2017;7(1):14696. https://doi.org/10.1038/s41598-017-14480-z, 9.
7. Levin JL, Rouk A, Shepherd S, et al. Tyler asbestos workers: A mortality update in a cohort exposed to amosite. *J Toxic Environ Health, Part B*. 2016;19(5–6):190-200. https://doi.org/10.1080/10937404.2016.1195319
8. Gilbert M. *Brydson's plastics materials*. Amsterdam: Butterworth-Heinemann; 2017.
9. Schiller JE, Payne SL, Khalafalla SE. Surface charge heterogeneity in amphibole cleavage fragments and asbestos fibers. *Science*. 1980;209(4464):1530-1532. https://doi.org/10.1126/science.209.4464.1530
10. Egilman D, Steffen JE, Tran T, et al. Health effects of censored elongated mineral particles: A critical review. In: Brisson M, ed. *Detection Limits in Air Quality and Environmental Measurements*. West Conshohocken, PA: ASTM International; 2019:192-239.
11. Woolhouse I, Bishop L, Darlison L, et al. British Thoracic Society guideline for the investigation and management of malignant pleural mesothelioma. *Thorax*. 2018;73:i1-i30. https://doi.org/10.1136/thoraxjnl-2017-211321
12. Korchevskiy A, Rasmuson JO, Rasmuson EJ. Empirical model of mesothelioma potency factors for different mineral fibers based on their chemical composition and dimensionality. *Inhal Toxicol*. 2019;31(5):180-191. https://doi.org/10.1080/08958378.2019.1640320
13. Jasani B, Gibbs A. Mesothelioma not associated with asbestos exposure. *Arch Pathol Lab Med*. 2012;136(3):262-267. https://doi.org/10.5858/arpa.2011-0039-RA
14. Dement JM, Kuempel ED, Zumwalde RD, Ristich AM, Fernback JE, Smith RJ. Airborne fiber size characterization in exposure estimation: Evaluation of a modified transmission electron microcopy protocol for asbestos and potential use for carbon nanotubes and nanofibers. *Am J Ind Med*. 2015;58(5):494-508. https://doi.org/10.1002/ajim.22422
15. Shimizu Y, Dobashi K, Kusakbe T, et al. In-air micro-particle induced X-ray emission analysis of asbestos and metals in lung tissue. *Int J Immunopathol Pharmacol*. 2008;21(3):567-576. https://doi.org/10.1177/039463200802100309
16. Pascolo L, Gianoncelli A, Kaulich B, et al. Synchrotron soft X-ray imaging and fluorescence microscopy reveal novel features of asbestos body morphology and composition in human lung tissues. *Part Fibre Toxicol*. 2011;8(1):7. https://doi.org/10.1186/1743-8977-8-7
17. Lee RF, Theiner S, Meibom A, Koellensperger G, Keppler BK, Dyson PJ. Application of imaging mass spectrometry approaches to facilitate metal-based anticancer drug research. *Metall: Integ Bio Sci*. 2017;9(4):365-381. https://doi.org/10.1039/c6mt00231e
18. Douglas DN, Managh AJ, Reid HJ, Sharp BL. High-speed, integrated ablation cell and dual concentric injector plasma torch for laser ablation-inductively coupled plasma mass spectrometry. *Anal Chem*. 2015;87(22):11285-11294. https://doi.org/10.1021/acs.analchem.5b02466
19. van Acker T, Buckle T, van Malderen SJM, et al. High-resolution imaging and single-cell analysis via laser ablation-inductively coupled plasma-mass spectrometry for the determination of membranous receptor expression levels in breast cancer cell lines using receptor-specific hybrid tracers. *Anal Chim Acta*. 2019;1074:43-53. https://doi.org/10.1016/j.aca.2019.04.064
20. van Malderen SJ, van Acker T, Vanhaecke F. Sub-micrometer nanosecond LA-ICP-MS imaging at pixel acquisition rates above 250 Hz via a low-dispersion setup. *Anal Chem*. 2020;92(8):5756-5764. https://doi.org/10.1021/acs.analchem.9b05056
21. Bulk M, Abdelmoula WM, Geut H, et al. Quantitative MRI and laser ablation-inductively coupled plasma-mass spectrometry imaging of iron in the frontal cortex of healthy controls and Alzheimer's disease patients. *Neuroimage*. 2020;215:116808.
22. Neumann B, Hösl S, Schwab K, Theuring F, Jakubowski N. Multiplex LA-ICP-MS bio-imaging of brain tissue of a parkinsonian mouse model stained with metal-coded affinity-tagged antibodies and coated with indium-spiked commercial inks as internal standards. *J Neurosci Methods*. 2020;334:108591. https://doi.org/10.1016/j.jneumeth.2020.108591
23. Pamphlett R, Satgunaseelan L, Kum Jew S, Doble PA, Bishop DP. Elemental bioimaging shows mercury and other toxic metals in normal breast tissue and in breast cancers. *PLoS ONE*. 2020;15(1):e0228226. https://doi.org/10.1371/journal.pone.0228226
24. Karekla E, Liao W, Sharp B, et al. Ex vivo explant cultures of non-small cell lung carcinoma enable evaluation of primary tumor responses to anticancer therapy. *Cancer Res*. 2017;77(8):2029-2039. https://doi.org/10.1158/0008-5472.CAN-16-1121
25. Pisonero J, Bouzas-Ramos D, Traub H, et al. Critical evaluation of fast and highly resolved elemental distribution in single cells using LA-ICP-SFMS. *J Anal At Spectrom*. 2019;34:655-663. https://doi.org/10.1039/C8JA00096D
26. Managh AJ, Douglas DN, Makella Cowen K, et al. Acquisition of fast transient signals in ICP-MS with enhanced time resolution. *J Anal At Spectrom*. 2016;31:1688-1692. https://doi.org/10.1039/c6ja00140h
27. Managh AJ, Reid P. A new freeware tool for image processing and its application to high speed LA-ICP-MS imaging. *J Anal At Spectrom*. 2019;34:1369-1373. https://doi.org/10.1039/c9ja00082h
28. May TW, Wiedmeyer RH. A table of polyatomic interferences in ICP-MS. *Atomic Spectrosc*. 1998;19:150-155.
29. Mohanty SK, Gonneau C, Salamatipour A, et al. Siderophore-mediated iron removal from chrysotile: Implications for asbestos toxicity reduction and bioremediation. *J Hazard Mater*. 2018;341:290-296. https://doi.org/10.1016/j.jhazmat.2017.07.033
30. Ishida T, Fujihara N, Nishimura T, et al. Live-cell imaging of macrophage phagocytosis of asbestos fibers under fluorescence microscopy. *Genes Environ*. 2019;41(1):1-11. https://doi.org/10.1186/s41021-019-0129-4
31. Pinkerton KE, Pratt PC, Brody AR, Crapo JD. Fiber localization and its relationship to lung reaction in rats after chronic inhalation of chrysotile asbestos. *Am J Pathol*. 1984;117(3):484-498.
32. Pascolo L, Gianoncelli A, Schneider G, et al. The interaction of asbestos and iron in lung tissue revealed by synchrotron-based scanning X-ray microscopy. *Sci Rep*. 2013;3(1):1-11. https://doi.org/10.1038/srep01123
33. Boulanger G, Andujar P, Pairon J, et al. Quantification of short and long asbestos fibers to assess asbestos exposure: A review of fiber size toxicity. *Environ Health*. 2014;13:59. https://doi.org/10.1186/1476-069x-13-59
34. Nagai H, Toyokuni S. Differences and similarities between carbon nanotubes and asbestos fibers during mesothelial carcinogenesis: Shedding light on fiber entry mechanism. *Cancer Sci*. 2012;103(8):1378-1390. https://doi.org/10.1111/j.1349-7006.2012.02326.x

How to cite this article: Voloaca OM, Greenhalgh CJ, Cole LM, Clench MR, Managh AJ, Haywood-Small SL. Laser ablation inductively coupled plasma mass spectrometry as a novel clinical imaging tool to detect asbestos fibres in malignant mesothelioma. *Rapid Commun Mass Spectrom*. 2020;34:e8906. https://doi.org/10.1002/rcm.8906